

Exploring the high-pressure behavior of superhard tungsten tetraboride

Miao Xie,¹ Reza Mohammadi,^{1,2} Zhu Mao,³ Matt M. Armentrout,³ Abby Kavner,^{3,*}
Richard B. Kaner,^{1,2,4,†} and Sarah H. Tolbert^{1,2,4,‡}

¹*Department of Chemistry and Biochemistry, University of California, Los Angeles, California 90095, USA*

²*Department of Materials Science and Engineering, University of California, Los Angeles, California 90095, USA*

³*Department of Earth and Space Sciences and Institute of Geophysics and Planetary Physics, University of California, Los Angeles, California 90095, USA*

⁴*California NanoSystems Institute (CNSI), University of California, Los Angeles, California 90095, USA*

(Received 19 August 2011; revised manuscript received 16 December 2011; published 24 February 2012)

In this work, we examine the high-pressure behavior of superhard material candidate WB₄ using high-pressure synchrotron x-ray diffraction in a diamond anvil cell up to 58.4 GPa. The zero-pressure bulk modulus, K_0 , obtained from fitting the pressure-volume data using the second-order Birch-Murnaghan equation of state is 326 ± 3 GPa. A reversible, discontinuous change in slope in the c/a ratio is further observed at ~ 42 GPa, suggesting that lattice softening occurs in the c direction above this pressure. This softening is not observed in other superhard transition metal borides such as ReB₂ compressed to similar pressures. Speculation on the possible relationship between this softening and the orientation of boron-boron bonds in the c direction in the WB₄ structure is included. Finally, the shear and Young's modulus values are calculated using an isotropic model based on the measured bulk modulus and an estimated Poisson's ratio for WB₄.

DOI: [10.1103/PhysRevB.85.064118](https://doi.org/10.1103/PhysRevB.85.064118)

PACS number(s): 64.30.-t, 81.05.Je

I. INTRODUCTION

The search for new superhard materials is driven by the need for chemically inert robust materials for abrasives, cutting tools, and coatings that can be synthesized under modest conditions. Broadly, two approaches are used to design and synthesize materials with high hardness. A first approach is to imitate natural diamond by combining light first-row elements (B, C, N, or O) to produce materials that maintain short bonds with high covalency, such as c -BN,¹ B₆O,² and BC₂N.³ A second route is to start with elemental metals that are intrinsically incompressible, but not hard, and try to improve their hardness by incorporating light elements into the metal structure to simultaneously optimize covalent bonding and valence-electron density.⁴ This class, which generally contains late, transition metal borides, carbides, nitrides, and oxides contains many candidate hard materials.^{5–8}

For example, by applying the second approach to Os, with a hardness of only 3.9 GPa, Cumberland *et al.*⁹ sought to introduce covalent bonds to its lattice using boron to increase its hardness, while maintaining the high bulk modulus. The presence of covalent bonds in OsB₂ results in a hardness of 21.6 GPa under an applied load of 0.49 N, without substantially reducing the bulk modulus (365–395 GPa).^{9,10} Although this hardness value is relatively high, it does not assign this material to the “superhard” category.¹¹ One reason for this is that the OsB₂ structure contains double Os layers, alternating with covalent B layers. The weak Os-Os metallic bonds within the layers likely reduce the resistance of OsB₂ to large shear deformations in the easy-slip direction, which is parallel to the layers.¹¹ To create potentially harder materials, hexagonal rhenium diboride was synthesized by completely replacing Re for Os. The ReB₂ structure consists of alternating single layers of hexagonally packed Re and puckered interconnected hexagonal rings of boron. Without the double metal layers that reduced the hardness for OsB₂, this material exhibits a much higher hardness of 48 ± 5.6 GPa under an applied load of 0.49 N.¹²

The next logical step in this pattern would be to further increase the boron concentration in a related late transition metal boride to further increase the hardness. Unfortunately, few transition metals form compounds with boron-to-metal ratios greater than 2:1. Tungsten, however, is an exception, forming the unusual compound tungsten tetraboride (WB₄). It is the highest boride formed under normal pressures.^{13–15} Interestingly, the structure of WB₄ exhibits a unique covalent bonding network with B-B covalent bonds aligned along the c -axis.¹⁶ This covalent bonding framework of WB₄ should result in a more isotropic structure than that exhibited by ReB₂. In general, isotropic structures favor high hardness, as demonstrated in diamond, because materials fail at the weakest point. This suggests that WB₄, embracing a more isotropic structure, has potential for improved hardness. As a candidate superhard material, WB₄ also has a number of advantages over other borides. Specifically, (1) both tungsten and boron are relatively inexpensive, (2) the lower metal content in the higher borides reduces the overall cost per volume of production, and (3) the higher boron content lowers the overall density of the compound, which could prove to be beneficial in applications where lightweight is a critical asset.¹⁷

Recently, Gu *et al.*¹⁸ synthesized WB₄, and they measured hardness values as high as 46.2 GPa and a bulk modulus of 304 ± 10 GPa by fitting the second-order Birch-Murnaghan equation of state (EOS). With an exceptionally high first derivative K_0' of 15.3 ± 5.7 , they obtained an extremely low value of the zero-pressure bulk modulus K_0 of 200 ± 40 GPa using the third-order Birch-Murnaghan EOS. Unfortunately, this work did not include any details on the synthesis of the WB₄ or present any raw x-ray diffraction data; thus, it is difficult to effectively evaluate the lattice behavior of WB₄ from this work, especially under extreme conditions. In parallel, Wang *et al.*¹⁶ theoretically predicted the hardness of WB₄ to be between 41.1–42.2 GPa with a bulk modulus of 292.7–324.3 GPa. They also calculated a low shear modulus of 103.6–181.6 GPa. More recently, Liu *et al.*¹⁹ studied the

high-pressure behavior of WB_4 synthesized using a hot press and compressed to 50.8 GPa with silicone oil as the pressure medium. The authors obtained values ranging from 256 to 342 GPa, depending on the EOS and the pressure range. Changing the pressure range can have a significant effect with silicone oil, because this pressure medium has a hydrostatic limit of 8 GPa²⁰ and develops a deviatoric stress of 1 GPa at pressures as low as 10 GPa.²¹ Nonhydrostaticity can result in strongly biased determination of elastic properties and also can result in diffraction peak broadening and loss of resolution that may mask small changes in the lattice parameter that indicate structural transitions. Thus, our current study aims to examine lattice behavior of WB_4 under more hydrostatic conditions, with a goal of resolving these conflicts in the value of bulk modulus.

In our recent study, high-quality crystalline WB_4 was successfully synthesized via arc melting. We confirmed the high hardness using both microindentation and nanoindentation, obtaining hardness values of 43.3 ± 2.9 GPa and 40.4 GPa, respectively.¹⁷ From high-pressure x-ray diffraction results, a bulk modulus of 339 ± 3 GPa was obtained using a second-order finite strain EOS. This value was 10% higher than the value reported by Gu *et al.*¹⁸ and was close to some of the value reported by Liu *et al.*¹⁹

In order to clarify the elastic moduli of WB_4 with higher accuracy and to further examine the lattice distortions of WB_4 under elevated pressure, we have undertaken a more complete experimental study of the pressure-dependent compression behavior of WB_4 using synchrotron-based angle-dispersive x-ray diffraction in the diamond anvil cell. It is now widely recognized that hydrostaticity is the key to obtaining reliable values of bulk modulus and its pressure derivatives, particularly for fairly incompressible materials. We have thus used neon as a pressure transmitting medium because it offers good quasihydrostatic conditions to at least 50 GPa.²⁰ In addition, we have performed a similar set of experiments on ReB_2 to 63 GPa, allowing us to compare and contrast the behavior of these two transition metal borides. The example of ReB_2 provides a good cross-comparison because of the close proximity of Re to W in the periodic table, the similar valence electron densities of these two materials (ReB_2 : $0.477 \text{ e}^- \text{ \AA}^{-3}$; WB_4 : $0.485 \text{ e}^- \text{ \AA}^{-3}$), the similar indentation hardness values measured for these materials (48.0 ± 5.6 GPa and 43.3 ± 2.9 GPa for ReB_2 ¹² and WB_4 ¹⁷, respectively), and their related structures (both with space group $P6_3/mmc$).

II. EXPERIMENTAL PROCEDURE

Powders of pure tungsten (99.9994%, JMC Puratronic, USA) and amorphous boron (99+%, Strem Chemicals, USA) were mixed together with a molar ratio of 1:11 and pressed into a pellet using a Carver press under 10 000 pounds of force. The pellets were then placed in an arc-melting furnace. The WB_4 ingot was synthesized by applying an ac current of >70 A under high-purity argon at ambient pressure. All ingots were crushed to form a fine powder using a hardened steel mortar and pestle set. The rhenium diboride sample was produced in a two-step process that involved first synthesizing ReB_2 powder and then sintering the powder into an ingot. The detailed description of the process can be found elsewhere.²²

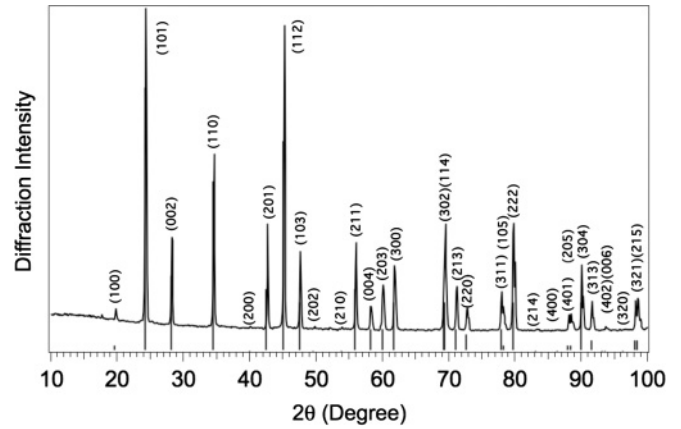


FIG. 1. Labeled x-ray diffraction pattern for powder tungsten tetraboride (WB_4) at ambient pressure (x-ray wavelength $\lambda=1.54 \text{ \AA}$). The vertical bars indicate previously determined lattice spacings for WB_4 (Joint Committee on Powder Diffraction Standards, Ref. code: 00-019-1373; Ref. 13). The corresponding Miller index is given above each peak. The material used in this work is thus shown to be highly crystalline and phase pure.

To confirm the phase purity of all powder samples, powder x-ray diffraction patterns were collected on an X'Pert ProTM x-ray powder diffraction system (PANalytical, Netherlands; Fig. 1). Elemental analysis was performed using a JSM-6700F field-emission scanning electron microscopy (JEOL Ltd.) equipped with an energy-dispersive x-ray spectroscopy detector (EDAX) using an ultrathin window.

High-pressure experiments were carried out using a symmetric diamond anvil cell equipped with 300- μm diamond culets using a preindented rhenium gasket with a 150- μm diameter sample chamber. A 50- μm diameter piece of sample was loaded into the cell, supported by a piece of platinum foil (5 μm thick, 99.95%, Alfa Aesar, USA), which was used as an internal pressure calibrant. We also placed a 10- μm ruby chip next to the sample as an external pressure calibrant. To ensure a quasihydrostatic sample environment, neon gas was loaded into the cell using the Consortium for Materials Properties Research in Earth Sciences (COMPRES) and GeoSoilEnviroCARS (GSECARS) gas-loading system.²³ High-pressure angle-dispersive x-ray diffraction experiments were performed on Beamline 12.2.2 at the Advanced Light Source (ALS, Lawrence Berkeley National Laboratory) and 16-BM-D of the High Pressure Collaborative Access Team (HPCAT) sector of the Advanced Photon Source (APS) with x-ray beam sizes of approximately $10 \times 10 \mu\text{m}^2$ and $5 \times 15 \mu\text{m}^2$, respectively. Image plate detectors were used at both beamlines. The distance and orientation of the detector were calibrated using LaB_6 and CeO_2 standards, respectively. Pressure was determined using ruby fluorescence. A secondary pressure calibration was performed by referencing the measured lattice parameter of the internal standard platinum (Pt) to its pressure-volume EOS. X-ray diffraction patterns of WB_4 and ReB_2 were collected up to pressures of 58.4 and 63 GPa, respectively.

III. RESULTS

At ambient temperature and pressure, x-ray diffraction studies of WB_4 reveal a hexagonal structure with the lattice

parameters $a = 5.1945 \pm 0.0013 \text{ \AA}$, $c = 6.3311 \pm 0.0030 \text{ \AA}$, and $V_0 = 147.94 \pm 0.15 \text{ \AA}^3$ and axial ratio $c/a = 1.2188 \pm 0.0006$ (Fig. 1). Representative high-pressure diffraction patterns for WB_4 are shown in Fig. 2. The two-dimensional diffraction patterns were integrated using the program FIT2D²⁴ to yield one-dimensional plots of x-ray intensity as a function of d -spacing. All patterns were indexed to the hexagonal phase, and there were no signs of phase transformations. The sample remained in the hexagonal phase up to the highest pressure of 58.4 GPa, at which point the lattice parameters were $a = 4.949 \pm 0.013 \text{ \AA}$ and $c = 5.984 \pm 0.027 \text{ \AA}$, and $V_0 = 126.9 \pm 1.30 \text{ \AA}^3$. Similarly, ReB_2 was also shown to be stable in the hexagonal phase to 63 GPa.

Figure 3 shows the normalized unit cell volume of WB_4 as a function of pressure, under both compression (filled circles) and decompression (open circles). Figure 4 shows the normalized compressibility of both the a - and c -lattice parameters of WB_4 . Up to ~ 40 GPa, both the a - and c -lattice constants show a gentle decrease upon compression, with the a -axis appearing slightly more compressible than the c -axis. However, at ~ 42 GPa, the c -axis appears to suddenly undergo a softening, becoming significantly more compressible than the a -axis. The a -axis does not show any change in behavior. This structural change is reversible, with the c -lattice constant recovering its original strain values upon decompression. This structural change has not been observed in other studies and emphasizes the need for high-quality data.

Because of this anomalous behavior in the c direction, fits to the Birch-Murnaghan EOS were performed at pressures lower than 42 GPa. The measured zero-pressure bulk modulus, K_0 , using a second-order Birch-Murnaghan EOS is 317 ± 3 GPa. Using a third-order Birch-Murnaghan EOS, we obtain values of $K_0 = 367 \pm 11$ GPa and $K_0' = 0.9 \pm 0.6$. Using only data obtained on compression results, we calculate $K_0 = 326 \pm 3$ GPa (second-order Birch-Murnaghan EOS) and $K_0 = 369 \pm 9$ GPa with $K_0' = 1.2 \pm 0.5$ (third-order

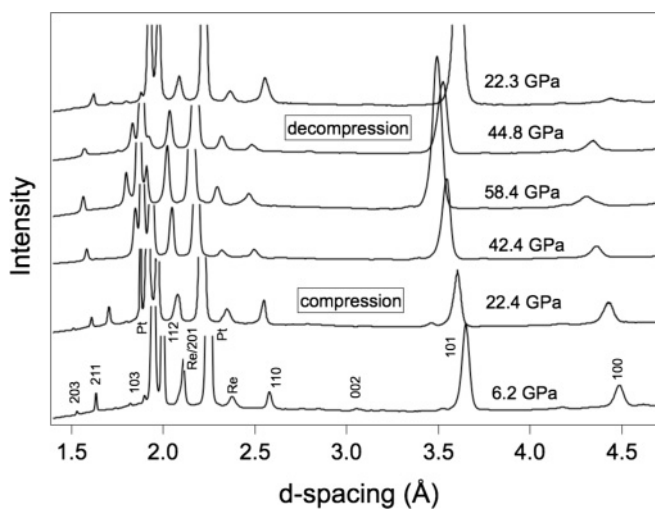


FIG. 2. Representative angle dispersive x-ray diffraction patterns for WB_4 as a function of increasing and decreasing pressure. The Re peaks are from the gasket due to incomplete filtering of the tails of the x-ray beam. No changes in peak patterns that would be indicative of a change in symmetry are observed under pressures up to 58.4 GPa.

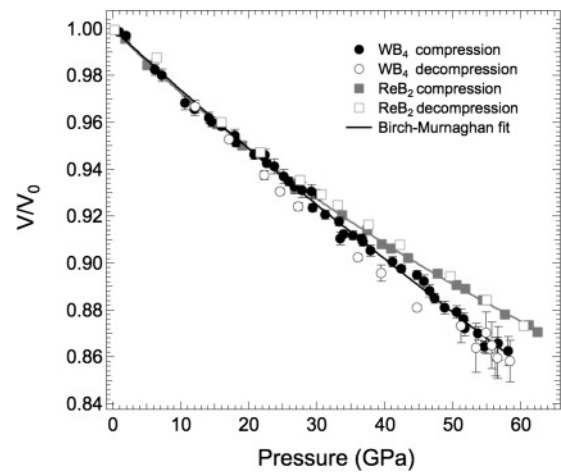


FIG. 3. Measured fractional unit cell volume of WB_4 and ReB_2 plotted as a function of pressure. Black solid circle: compression of WB_4 ; black open circle: decompression of WB_4 ; gray solid square: compression of ReB_2 ; gray open square: decompression of ReB_2 ; black solid line: a Birch-Murnaghan fit to the compression data of WB_4 ; and gray solid line: a Birch-Murnaghan fit to the compression data of ReB_2 . Error bars that are smaller than the size of the symbol have been omitted. While WB_4 is more compressible than ReB_2 under high pressures, below 30 GPa the data are quite comparable.

Birch-Murnaghan EOS). The second-order values are slightly lower than our previous study of WB_4 , which presented a bulk modulus of 339 ± 3 GPa obtained using a second-order finite strain EOS.¹⁷ The inferred values of K_0 and $(dK/dP)_0$ are strongly correlated, however, with an inverse relationship. For the WB_4 data up to 40 GPa, the pairs $(K_0, K_0') = (326, 4)$

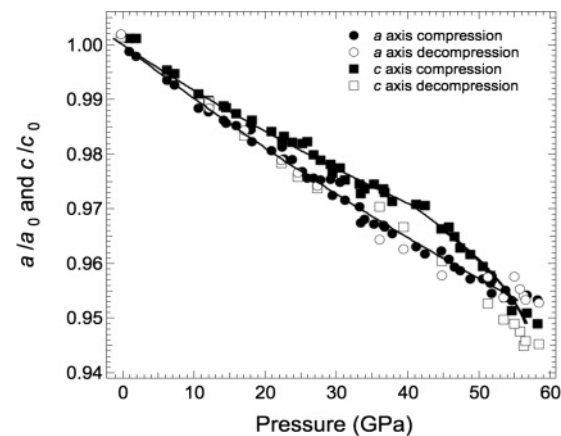


FIG. 4. WB_4 fractional lattice parameters plotted as a function of pressure. Black solid circles: compression data for the a -lattice constant; black open circle: decompression data for the a -lattice constant; black solid squares: compression data for the c -lattice constant; black open square: decompression for the c -lattice constant; and solid lines: fits to the Birch-Murnaghan EOS. The error bars when not shown are smaller than the symbol. At ~ 42 GPa during compression, the c -lattice constant undergoes a softening and becomes more compressible than the a -lattice constant. The a -lattice constant does not exhibit this abrupt change. Decompression data reveal that this structural change is reversible but with some hysteresis.

TABLE I. Comparison of the theoretical calculations and experimental results for the bulk modulus K_0 (GPa) and their first derivative K_0' , shear modulus G (GPa), Young's modulus E (GPa), and Poisson's ratio ν of WB_4 and ReB_2 found in the literature and presented in this study.

Material			K_0	K_0'	G	E	ν
ReB_2	Cal.	Wang (LDA) ^a Ref. 27	359		313	696	0.22
		Wang (GGA) ^a Ref. 27	344		304	642	0.21
		Hao <i>et al.</i> (LDA) Ref. 28	369.2		294.9	698.7	0.1846
		Hao <i>et al.</i> (GGA) Ref. 28	354.5		289.4	682.5	0.1791
		Chung <i>et al.</i> (x-ray) Refs. 12, 29	360 ^b	4		712	
	Expt.	Levine <i>et al.</i> (RUS) Ref. 22	383 ^c		273	661	0.21
		Koehler <i>et al.</i> (RUS) Ref. 25	317 ^c		276	642	0.163
		Suzuki <i>et al.</i> (RUS) Ref. 26	367.7 ^c		271.6	671.2	0.1958
		This work	344 ^b	4			
		This work	340 ^b	4.2			
WB_4	Cal.	Wang <i>et al.</i> (GGA) Ref. 16	292.7		103.6		
		Wang <i>et al.</i> (LDA) Ref. 16	324.3		129.1		
		Mohammadi <i>et al.</i> Ref. 17 (x-ray)	339 ^b	4	553.8		
	Expt.	Gu <i>et al.</i> Ref. 18 (x-ray)	304 ^b	4			
		Liu <i>et al.</i> Ref. 19 (x-ray)	200 ^b	15.3			
		Liu <i>et al.</i> Ref. 19 (x-ray)	342 ^b	4			
		This work	325 ^b	5.1			
		This work	326 ^b	4	249	595	
This work	369 ^b	1.2					

^aGGA refers to the generalized gradient approximation; LDA refers to local density approximation.

^bReported bulk modulus K_0 are isothermal values. Measured bulk modulus is obtained by fitting Birch-Murnaghan EOS.

^cReported bulk moduli are adiabatic values.

and (369, 1.2) are statistically indistinguishable. The trade-offs between the two parameters are plotted in Fig. 6, which shows contours for the sum of the deviations from the fits as a function of varying K_0 and K_0' . The trade-off between K_0 and K_0' produces a change in bulk modulus of -12 GPa for every 1 of K_0' WB_4 . This relationship is sufficient to explain the variation in previous studies, including the exceptional low-bulk modulus in Gu's results.¹⁸

Figure 3 also shows the compression and decompression behavior of ReB_2 up to 63 GPa. Second-order Birch-Murnaghan equation fitting to the ReB_2 data gives an ambient bulk modulus of $K_0 = 344 \pm 1$ GPa, with a similar trade-off between K_0 and $(dK/dP)_0$ (Fig. 6). The measured bulk modulus is slightly lower than the previously reported bulk modulus of 360 GPa, also obtained using second-order Birch-Murnaghan EOS fits to pressure-dependent x-ray diffraction,¹² but both values fall in the range of 317–383 GPa, previously reported from resonant ultrasound spectroscopy (RUS) experiments (Table I).^{22,25–29} Fitting the third-order Birch-Murnaghan EOS gives $K_0 = 340 \pm 5$ GPa with $K_0' = 4.2 \pm 0.2$. Compressibility

along different crystallographic axes in hexagonal ReB_2 is illustrated in Fig. 5. Importantly, close examination of a - and c -lattice constants shows no evidence of lattice softening in either direction. Comparison of Figs. 4 and 5 also clearly emphasizes that WB_4 shows much more isotropic bonding than ReB_2 with much more similar compressibility in a and c directions.

IV. DISCUSSION

At the point of the structural change at 42 GPa, the WB_4 diffraction pattern remains the same, with no evidence of peak broadening or splitting (Fig. 2). Thus, there is no evidence for a first-order phase transition. Additionally, the compression behavior is reversible upon release of pressure. Because this transition pressure for WB_4 (42 GPa) appears far from the hydrostatic limit of the pressure medium (~ 15 GPa),²⁰ it is unlikely that deviation from hydrostaticity is responsible for this observation. Additionally, if deviatoric stresses were affecting the measured x-ray strains, the axial geometry

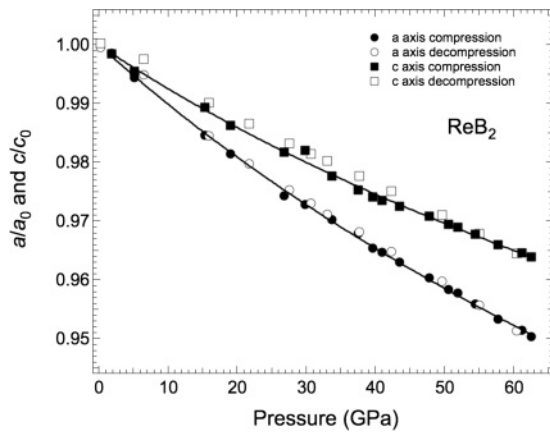


FIG. 5. ReB_2 fractional lattice parameters plotted as a function of pressure. Black solid circles: compression data for the a -lattice constant; black open circle: decompression data for the a -lattice constant; black solid squares: compression data for the c -lattice constant; black open square: decompression for the c -lattice constant; and solid lines: fits to the Birch-Murnaghan EOS. Examination of the a - and c -lattice constants shows no evidence of lattice softening in either direction during compression.

of the x-ray in the diamond anvil cell combined with the gasket direction would predict the opposite observation—that lattice planes should appear less compressible, not more compressible, as the medium becomes less hydrostatic. As a result, it appears that the abrupt change in c/a ratio observed at 42 GPa is a real structural change of the system; specifically, a second-order phase transition. The challenge now is to understand the origins of this phase transition and to determine if it can provide insight into the bonding found in this unique metal tetraboride.

To make a more direct comparison between the high-pressure behavior of WB_4 and ReB_2 , we examined their c/a ratios normalized to each other at ambient pressure. Because the unit cells are not the same in these two materials, the absolute c/a ratios are rather different (1.2188 for WB_4 and 2.5786 for ReB_2 ; Fig. 7). Normalization is thus required to compare the fairly small changes observed here. Up to ~ 40 GPa, both materials show a linear increase in their c/a ratio of similar magnitude. However, this increase continues for ReB_2 while there is a discontinuous change in slope for the c/a ratio at ~ 42 GPa for WB_4 . As shown in Fig. 4, this c/a ratio drop can be almost solely accounted for by the anomalous compression behavior of the c -axis.

This structural change may be mechanical or may be electronic in nature. Electronic band structure calculations has been reported on ReB_2 without any evidence for transitions up to 90 GPa,³⁰ but less is known for WB_4 . Although transitions based on changes in optimal atomic positions or bond orientation may seem to be the likely explanation for the observed transitions, other anomalous compression phenomena have been documented experimentally^{31–34} and theoretically^{35–43} when distortion of the electronic band structure results in a topological singularity of the Fermi surface. Those are known as electronic topological transitions (ETTs) or Lifshitz transitions.⁴⁴ The anomaly has mostly been found in hexagonal-close-packed (hcp) metals, including

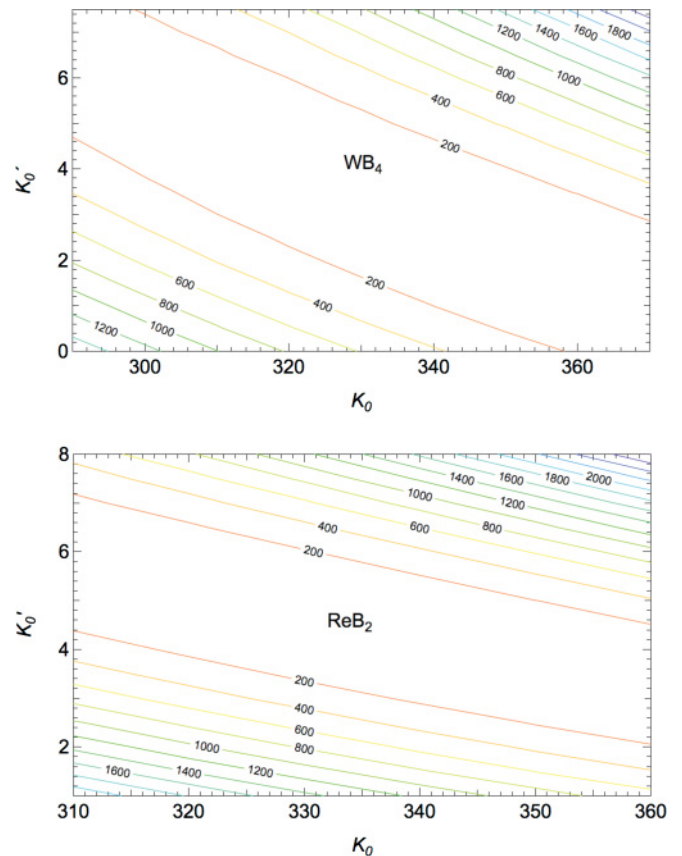


FIG. 6. (Color online) Trade-off of zero-pressure bulk modulus K_0 and its first derivative K_0' for WB_4 and ReB_2 . The contours are the sum of the deviations from the fits as a function of varying K_0 and K_0' . The inferred values of K_0 and K_0' have an inverse relationship. The value obtained from second- or third-order Birch-Murnaghan EOS cannot be statistically distinguished based on this analysis.

Zn ,^{31–34} Cd ,³¹ and Os ,^{46,47} and intermetallic compounds such as AuIn_2 ^{42,43} or $\text{Cd}_{0.8}\text{Hg}_{0.2}$.⁴⁵ However, these transitions are highly controversial because of their subtle nature and because of difficulties in their direct experimental detection at high pressures. The magnitude of the anomalies observed in the compression data associated with ETTs is usually small, as opposed to the significant softening observed in WB_4 . In addition, most of the discontinuities associated with electronic phase transition occur below 20 GPa (e.g., calculated to be 7 and 14 GPa for Zn ⁴⁰; observed at 2.7 GPa for AuIn_2 ^{42,43}). Moreover, ETTs do not necessarily affect only one lattice direction and usually result in a decrease in compressibility after the anomaly. Although the possibility of an ETT in WB_4 at high pressure is intriguing, the data do not fit the standard profile for these transitions, and thus it seems likely that the observed bond softening in WB_4 does not arise from this kind of singularity but is instead due to changes in optimal bonding at high pressure.

Lacking the observation of peak splitting and/or a new phase in the x-ray diffraction data, we assign this anomaly to a structurally induced second-order phase transition. The intersection of the two regions defines the transition pressure at 42 GPa. Furthermore, Fig. 7 reveals that although the c/a compression behavior is reversible, the c/a ratio does not fully

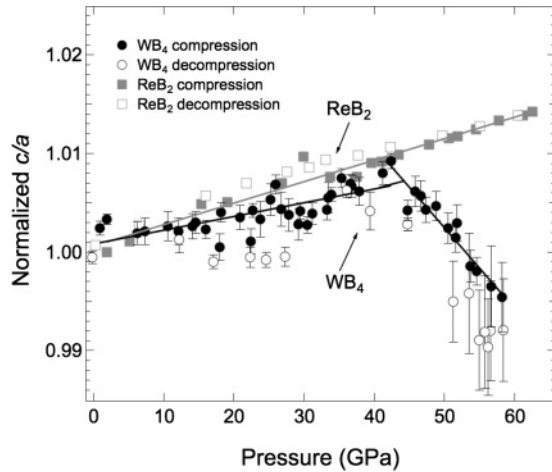


FIG. 7. Normalized c/a ratio plotted as a function of pressure for WB_4 and ReB_2 . Black solid circle: compression of WB_4 ; black open circle: decompression of WB_4 ; gray solid square: compression of ReB_2 ; gray open square: decompression of ReB_2 ; and solid lines: linear fits of compression data serve as a guide to the eye. WB_4 undergoes a pressure-induced second-order phase transition at ~ 42 GPa. This transition is reversible with some hysteresis, suggesting a mechanical origin. In contrast, ReB_2 shows no evidence of a phase transition. The different pressure behavior can be related to difference in crystal structures between these two materials.

recover its compression value until the pressure is decreased to less than 20 GPa. Such hysteresis further indicates that the softening is mechanical, rather than electronic in origin.

In order to understand this decompression behavior, the nature of the second-order phase transition of WB_4 , and the lack of similar pressure-induced lattice-axis softening in ReB_2 and OsB_2 , it is essential to consider the crystal structures of both ReB_2 and WB_4 [Figs. 8(a) and 8(b)]. The crystal structure of ReB_2 [Fig. 8(a)] is characterized by alternating layers of metal atoms and boron atoms. The boron atoms are condensed into six-membered rings in a chairlike conformation. The Re atoms are arranged in a hcp layer with B atoms occupying all tetrahedral voids; this enlarges the lattice by about 40%. A strong anisotropy has been found in the hexagonal structure (Fig. 5), with the c -axis much less compressible than the a -axis. This can be explained by the directional electronic

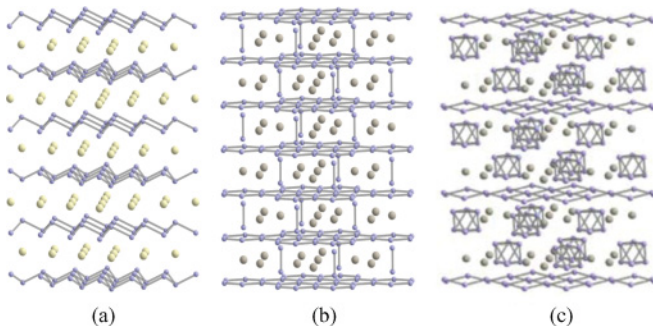


FIG. 8. (Color online) (a) Crystal structure of ReB_2 , (b) suggested structure of WB_4 , and (c) a second suggested structure for WB_4 ($W_{1.83}B_9$). The presence of the boron-boron covalent bonds in WB_4 may account for its distinct high-pressure behavior relative to ReB_2 .

repulsion between the borons and transition metal atoms aligned along the c -axis. This repulsion reduces the pressure-induced compression in the c direction. Because the layers are not highly constrained in the a - b direction, continuous structural optimization upon compression results in smooth and continuous changes in the c -axis lattice constant up to 63 GPa.

The most widely cited structure of WB_4 was originally assigned by Romans and Krug in 1966,¹³ which consists of alternating hexagonal layers of boron and tungsten atoms [Fig. 8(b)]. In contrast with the ReB_2 structure [Fig. 8(a)], however, these planar B layers are propped up by B-B bonds aligned along the c -axis. This could make the c direction more compressible (pure B is more compressible than ReB_2) and less flexible. We hypothesize that because of the more constrained bonding in the WB_4 structure, high-pressure bond optimization within the ambient-pressure structure may be difficult, and a second-order phase transition could be required to optimize the bonding at high pressure. This would not be the case for the less constrained ReB_2 structure, which shows no signs of phase transitions up to 63 GPa. Upon decompression, the structural distortion is recovered, but rather incomplete at a low pressure, as is typical for pressure-induced phase transitions.

Note that at least one competing, although lesser known, structure has been proposed for WB_4 [Fig. 8(c)].⁴⁸ Although the tungsten lattice remains the same, there are considerable stoichiometric variations (WB_4 vs $W_{1.83}B_9$) and boron lattice dissimilarities between the two structures. The unresolved structure certainly warrants more investigation, but for this discussion, the differences may not be that important as both structures contain a three-dimensional boron network, including both boron layers in the a - b plane and boron covalent bonding in the c direction.

Because the primary interest in both ReB_2 and WB_4 is for applications as hard materials, the structural insights gained by examining lattice behavior under high-pressure conditions may be used to establish design parameters for developing new superhard materials. In order for a solid to have a high hardness, it must possess sufficient structural integrity that can survive large shear strains without collapse.⁴⁹ A strongly covalently bonded three-dimensional and isotropic network may ensure high intrinsic hardness of a material, as seen in diamond and c -BN.⁵⁰ In WB_4 , the presence of strong covalent B-B bonds in the c -axis apparently adds three-dimensional rigidity to the structure, which could reduce the chances of shear deformation or the creation and motion of the dislocations. At the same time, this three-dimensional boron bonding could create a more isotropic bonding environment that can potentially withstand larger shear strains.

Moreover, high-pressure x-ray absorption spectroscopy on ReB_2 has shown flattening of the boron layers with increasing hydrostatic pressures.⁵¹ The flattening should facilitate slipping of the layers in the a - b plane and further reduce the hardness under load. Therefore, it may be that WB_4 possesses a higher resistance to shear strain and less dislocation activity compared to ReB_2 because of its three-dimensional, almost isotropic covalently bonded network. Although WB_4 is more compressible than ReB_2 , it is intrinsically as hard, if not harder, than ReB_2 . While the pressure-induced bond softening observed here is not a cause of this increased hardness; it is

likely that the structural change observed in WB_4 , but not in ReB_2 , and the comparatively high hardness of WB_4 both stem from the increased stiffness of WB_4 that arises from the three-dimensional boron network.

Many attempts have been made to correlate hardness with other physical properties for a wide range of hard materials, especially bulk modulus and shear modulus.^{4,9,12,29,52–65} Shear modulus is generally a much better predictor of hardness than bulk modulus.^{52–58} We thus present here a calculated shear modulus of WB_4 , obtained from the bulk modulus and an estimated Poisson's ratio using an isotropic model. We begin the estimation by assuming WB_4 has little elastic anisotropy, as demonstrated in OsB_2 ²⁷ and ReB_2 ,²⁸ so that an isotropic model can be applied. Because the Poisson's ratio of WB_4 has not yet been experimentally measured, the recently reported value of 0.1958 for ReB_2 from resonant ultrasound spectroscopy is used.²⁶ An isotropic model is then applied to estimate the shear modulus and the Young's modulus based on the measured bulk modulus and estimated Poisson's ratio of WB_4 . The calculated shear and Young's modulus values are compared with first-principles calculations and nanoindentation data in Table I. The measured bulk modulus (326 GPa) is in excellent agreement with the first-principles calculations based on the LDA method (324 GPa)¹⁶ and falls between Gu *et al.*¹⁸ and our previous x-ray diffraction data.¹⁷ Our shear modulus derived from the isotropic model is 249 GPa, comparable with the measured shear modulus of ReB_2 (223–276 GPa)^{22,25} and nearly twice the value reported from theoretical calculations (104–129 GPa).¹⁶ Although many assumptions went into calculating this shear modulus, the high value seems reasonable given the similar hardnesses of ReB_2 and WB_4 and the known correlation between shear modulus and hardness. Finally, the Young's modulus calculated from the bulk modulus in a similar manner to the shear modulus is 595 GPa, which is only slightly higher than the value of 553.8 GPa derived from nanoindentation measurements¹⁷ but lower than the measured Young's modulus of ReB_2 (642–671 GPa).²⁹

V. CONCLUSIONS

WB_4 and ReB_2 were studied using synchrotron x-ray diffraction under quasihydrostatic conditions up to 58.4 and

63 GPa, respectively. In contrast to ReB_2 , we found an anomalous lattice softening of the *c*-axis in WB_4 during compression, which was partially reversible during decompression. The anomaly was assigned to a second-order phase transition and may be due to pressure-induced structural rearrangements that are required because of the more rigid nature of the WB_4 network, compared with ReB_2 . We believe that the three-dimensional, almost isotropic, rigid covalently boron network in WB_4 is responsible for both the observed structural change in WB_4 and its high intrinsic hardness. In addition, based on our measured bulk modulus and an estimated Poisson's ratio, a high shear modulus of 249 GPa was estimated for WB_4 using an isotropic model.

By examining the behavior of superhard materials like WB_4 under extreme conditions such as highly elevated pressures, we begin to understand the structural change that take place in these strongly bonded solids. In this way, we build up a knowledge base so that future iterations of ultra-incompressible superhard materials can be produced by design, rather than by the trial-and-error process that we are often forced to employ.

ACKNOWLEDGMENTS

The authors thank Andrew T. Lech and Beth E. Weaver for their assistance in experiments. This work was funded by the National Science Foundation (NSF) under Grants No. DMR-0805357 and No. DMR-1106364 (S.H.T. and R.B.K.). Portions of this work were performed at the ALS, Lawrence Berkeley National Laboratory. The Advanced Light Source is supported by the Director, Office of Science, Office of Basic Energy Sciences (BES), of the US Department of Energy (DOE) under Contract No. DE-AC02-05CH11231. Portions of this work were performed at the HPCAT (Sector 16) and GeoSoilEnviroCARS (Sector 13), APS, Argonne National Laboratory. HPCAT is supported by DOE-BES, DOE-National Nuclear Security Administration, NSF, and the W. M. Keck Foundation. GSECARS is supported by NSF, under Contract EAR-0622171 and DOE (DE-FG02-94ER14466). APS is supported by DOE-BES under Contract No. DE-AC02-06CH11357.

*akavner@ucla.edu

†kaner@chem.ucla.edu

‡tolbert@chem.ucla.edu

¹T. Taniguchi, M. Akaiishi, and S. Yamaoka, *J. Am. Ceram. Soc.* **79**, 547 (1996).

²D. W. He, Y. S. Zhao, L. Daemen, J. Qian, T. D. Shen, and T. W. Zerda, *Appl. Phys. Lett.* **82**, 643 (2002).

³V. L. Solozhenko, D. Andrault, G. Fiquet, M. Mezouar, and D. C. Rubie, *Appl. Phys. Lett.* **78**, 1385 (2001).

⁴R. B. Kaner, J. J. Gilman, and S. H. Tolbert, *Science* **308**, 1268 (2005).

⁵J. S. Tse, D. D. Klug, K. Uehara, Z. Q. Li, J. Haines, and J. M. Léger, *Phys. Rev. B* **61**, 10029 (2000).

⁶H. C. Lee and J. Gurland, *Mater. Sci. Eng.* **33**, 125 (1978).

⁷A. Zerr, G. Miehe, and R. Riedel, *Nat. Mater.* **2**, 185 (2003).

⁸D. S. Stone, K. B. Yoder, and W. D. Sproul, *J. Vac. Sci. Technol. A* **9**, 2543 (1991).

⁹R. W. Cumberland, M. B. Weinberger, J. J. Gilman, S. M. Clark, S. H. Tolbert, and R. B. Kaner, *J. Am. Chem. Soc.* **127**, 7264 (2005).

¹⁰H.-Y. Chung, J. M. Yang, S. H. Tolbert, and R. B. Kaner, *J. Mater. Res.* **23**, 1797 (2008).

¹¹J. Yang, H. Sun, and C. Chen, *J. Am. Chem. Soc.* **130**, 7200 (2008).

¹²H.-Y. Chung, M. B. Weinberger, J. B. Levine, A. Kavner, J.-M. Yang, S. H. Tolbert, and R. B. Kaner, *Science* **316**, 436 (2007).

¹³P. A. Romans and M. P. Krug, *Acta Crystallogr.* **20**, 313 (1966).

- ¹⁴L. G. Bodrova, M. S. Kovalchenko, and T. I. Serebryakova, *Powder Metall. Met. Ceram.* **13**, 1 (1974).
- ¹⁵H. Itoh, T. Matsudaira, S. Naka, H. Hamamoto, and M. Obayashi, *J. Mater. Sci.* **22**, 2811 (1987).
- ¹⁶M. Wang, Y. Li, T. Cui, Y. Ma, and G. Zou, *Appl. Phys. Lett.* **93**, 101905 (2008).
- ¹⁷R. Mohammadi, A. T. Lech, M. Xie, B. E. Weaver, M. T. Yeung, S. H. Tolbert, and R. B. Kaner, *Proc. Nat. Acad. Sci. USA* **108**, 10959 (2011).
- ¹⁸Q. Gu, G. Krauss, and W. Steurer, *Adv. Mater.* **20**, 3630 (2008).
- ¹⁹C. Liu, F. Peng, N. Tan, J. Liu, F. Lia, J. Qin, J. Wang, Q. Wang, and D. He, *High Press. Res.* **31**, 2 (2011).
- ²⁰S. Klotz, J.-C. Chervin, P. Munsch, and G. Le Marchand, *J. Phys. D* **42**, 075413 (2009).
- ²¹J. Zhao, R. J. Angel and N. L. Ross, *J. Appl. Crystallogr.* **43**, 743 (2010).
- ²²J. B. Levine, J. B. Betts, J. D. Garrett, S. Q. Guo, J. T. Eng, A. Migliori, and R. B. Kaner, *Acta Mater.* **58**, 1530 (2010).
- ²³M. Rivers, V. B. Prakapenka, A. Kubo, C. Pullins, C. M. Holl, and S. D. Jacobsen, *High Press. Res.* **28**, 273 (2008).
- ²⁴A. Hammersley, S. Svensson, M. Hanfland, A. Fitch, and D. Hausermann, *High Press. Res.* **14**, 235 (1996).
- ²⁵M. R. Koehler, V. Keppens, B. C. Sales, R. Y. Jin, and D. Mandrus, *J. Phys. D* **42**, 095414 (2009).
- ²⁶Y. Suzukia, J. B. Levine, A. Migliori, J. D. Garrett, R. B. Kaner, V. R. Fanelli, and J. B. Betts, *J. Acoust. Soc. Am.* **127**, 2797 (2010).
- ²⁷Y. X. Wang, *Appl. Phys. Lett.* **91**, 101904 (2007).
- ²⁸X. F. Hao, Y. H. Xu, Z. J. Wu, D. F. Zhou, X. J. Liu, X. Q. Cao, and J. Meng, *Phys. Rev. B* **74**, 224112 (2006).
- ²⁹H.-Y. Chung, M. B. Weinberger, J. M. Yang, S. H. Tolbert, and R. B. Kaner, *Appl. Phys. Lett.* **92**, 261904 (2008).
- ³⁰E. Zhao, J. Wang, J. Meng, and Z. Wu, *J. Comput. Chem.* **31**, 1904 (2010).
- ³¹T. Kenichi, *Phys. Rev. B* **56**, 5170 (1997).
- ³²T. Kenichi, *Phys. Rev. Lett.* **75**, 1807 (1995).
- ³³O. Schulte and W. B. Holzapfel, *Phys. Rev. B* **53**, 569 (1996).
- ³⁴T. Kenichi, *Phys. Rev. B* **60**, 6171 (1999).
- ³⁵S. Meenakshi, V. Vijayakumar, B. K. Godwal, and S. K. Sikka, *Phys. Rev. B* **46**, 14359 (1992).
- ³⁶B. K. Godwal, S. Meenakshi, and R. S. Rao, *Phys. Rev. B* **56**, 14871 (1997).
- ³⁷D. L. Novikov, M. I. Katsnelson, A. V. Trefilov, A. J. Freeman, N. E. Christensen, A. Svane, and C. O. Rodriguez, *Phys. Rev. B* **59**, 4557 (1999).
- ³⁸G. Steinle-Neumann, L. Stixrude, and R. E. Cohen, *Phys. Rev. B* **63**, 054103 (2001).
- ³⁹B. K. Godwal, P. Modak, and R. S. Rao, *Solid State Commun.* **125**, 401 (2003).
- ⁴⁰S. L. Qiu, F. Apostol, and P. M. Marcus, *J. Phys. Condens. Matter* **16**, 6405 (2004).
- ⁴¹G. V. Sin'ko and N. A. Smirnov, *J. Phys. Condens. Matter* **17**, 559 (2005).
- ⁴²B. K. Godwal, A. Jayaraman, S. Meenakshi, R. S. Rao, S. K. Sikka, and V. Vijayakumar, *Phys. Rev. B* **57**, 773 (1998).
- ⁴³B. K. Godwal, S. Speziale, S. M. Clark, J. Yan, and R. Jeanloz, *J. Phys. Chem. Solids* **71**, 1059 (2010).
- ⁴⁴I. M. Lifshitz, *Sov. Phys. JETP* **11**, 1130 (1960).
- ⁴⁵S. Speziale, R. Jeanloz, S. M. Clark, S. Meenakshi, V. Vijayakumar, A. K. Verma, R. S. Rao, and B. K. Godwal, *J. Phys. Chem. Solids* **69**, 2325 (2008).
- ⁴⁶F. Occelli, D. L. Farber, J. Badro, C. M. Aracne, D. M. Teter, M. Hanfland, B. Canny, and B. Couzinet, *Phys. Rev. Lett.* **93**, 095502 (2004).
- ⁴⁷D. Koudela, M. Richter, A. Möbius, K. Koepf, and H. Eschrig, *Phys. Rev. B* **74**, 214103 (2006).
- ⁴⁸H. Nowotny, H. Haschke, and F. Benesovsky, *Monatsh. Chem.* **98**, 547 (1967).
- ⁴⁹S. Veprek, A. S. Argon, and R. F. Zhang, *Philos. Mag.* **90**, 4101 (2010).
- ⁵⁰S. Veprek, *J. Vac. Sci. Technol. A* **17**, 2401 (1999).
- ⁵¹J. Pellicer-Porres, A. Segura, A. Muñoz, A. Polian, and A. Congeduti, *J. Phys. Condens. Matter* **22**, 045701 (2010).
- ⁵²J. J. Gilman, R. W. Cumberland, and R. B. Kaner, *Int. J. Refract. Met. Hard Mater.* **24**, 1 (2006).
- ⁵³V. V. Brazhkin, A. G. Lyapin, and R. J. Hemley, *Philos. Mag. A* **82**, 231 (2001).
- ⁵⁴N. Dubrovinskaia, L. Dubrovinsky, W. Crichton, F. Langenhorst, and A. Richter, *Appl. Phys. Lett.* **87**, 831061 (2005).
- ⁵⁵N. Dubrovinskaia, L. Dubrovinsky, and V. L. Solozhenko, *Science* **318**, 1550c (2007).
- ⁵⁶J. S. Tse, *J. Superhard Mater.* **32**, 177 (2010).
- ⁵⁷A. P. Gerk, *J. Mater. Sci.* **12**, 735 (1977).
- ⁵⁸D. M. Teter, *MRS Bull.* **23**, 22 (1998).
- ⁵⁹J. J. Gilman, *Electronic Basis of the Strength of Materials* (Cambridge University Press, Cambridge, 2003).
- ⁶⁰C. M. Sung and M. Sung, *Mater. Chem. Phys.* **43**, 1 (1996).
- ⁶¹J. Haines, J. M. Leger, and G. Bocquillon, *Annu. Rev. Mater. Res.* **31**, 1 (2001).
- ⁶²J. M. Leger, J. Haines, M. Schmidt, J. P. Petit, A. S. Pereira, and J. A. H. Dajornada, *Nature (London)* **383**, 401 (1996).
- ⁶³A. Y. Liu and M. L. Cohen, *Science* **245**, 841 (1989).
- ⁶⁴V. V. Brazhkin, A. G. Lyapin, and R. J. Hemley, *Philos. Mag.* **82**, 231 (2002).
- ⁶⁵A. R. Oganov and A. O. Lyakhova, *J. Superhard Mater.* **32**, 143 (2010).